Journal of Materials Chemistry A

A small molecule donor containing non-fused ring core for all-small-molecule organic solar cells with high efficiency over 11%

Journal:	*Journal of Materials Chemistry A*
Manuscript ID	TA-ART-11-2018-011441.R1
Article Type:	Paper
Date Submitted by the Author:	10-Jan-2019
Complete List of Authors:	Li, Xinxin; Soochow University, Wang, Yan; Laboratory of Advanced Optoelectronic Materials, College of Chemistry, Chemical Engineering and Materials Science, Soochow University Guo, Xia; Soochow University, Laboratory of Advanced Optoelectronic Materials, College of Chemistry, Chemical Engineering and Materials Science Zhu, Qinglian; Xi'an Jiaotong University, State Key Laboratory for Mechanical Behavior of Materials Ma, Wei; Xi'an Jiaotong University, State Key Laboratory for Mechanical Behavior of Materials Ou, Xuemei; Soochow University Zhang, Maojie; Soochow University, Laboratory of Advanced Optoelectronic Materials, College of Chemistry, Chemical Engineering and Materials Science Li, Yongfang; Chinese Academy of Sciences, Institute of Chemistry

A small molecule donor containing non-fused ring core for all-small-molecule organic solar cells with high efficiency over 11%

Xinxin Li[a], Yan Wang[a], Qinglian Zhu[b], Xia Guo[a], Wei Ma[b], Xuemei Ou[a], Maojie Zhang[a],* Yongfang Li[ac]

[a] *Laboratory of Advanced Optoelectronic Materials, College of Chemistry, Chemical Engineering and Materials Science, Soochow University, Suzhou 215123, China.*

E-mail: mjzhang@suda.edu.cn

[b] *State Key Laboratory for Mechanical Behavior of Materials, Xi'an Jiaotong University, Xi'an 710049, China.*

[c] *CAS Research/Education Center for Excellence in Molecular Sciences, CAS Key Laboratory of Organic Solids, Institute of Chemistry, Chinese Academy of Sciences, Beijing 100190, China.*

Abstract: A novel *p*-type organic semiconductor (*p*-OS) P2TBR, based on non-fused ring structure of thiophene-benzene-thiophene (TBT) as core and 2D-conjugated benzodithiophene (BDT) unit as π spacers and 3-ethylrhodanines as terminal groups, was synthesized and used as the donor material for all-small molecule organic solar cells (SM-OSCs). P2TBR shows strong absorption, low-lying HOMO energy level, high hole mobility and good thermal stability. The optimized P2TBR:IDIC film has a face-on and edge-on co-existent texture and three dimensional (3D) charge pathways, which is far better than that of the face-on orientated blend film without any treatment. As a result, a notable power conversion efficiency (PCE) of 11.5% and a satisfactory fill factor (FF) of 70.1% is achieved.

This efficiency is the highest PCE for non-fullerene SM-OSCs reported in the literature so far. Overall, the results indicate that P2TBR is a promising candidate of *p*-OS donor materials in SM-OSCs, and the molecular design strategy for P2TBR gives a guideline that the simple-structured and easy chemical modification non-fused unit can be also used as building blocks in high performance *p*-OS donors.

Introduction

Solution-processed organic solar cells (OSCs) with bulk heterojunction (BHJ) structures have attracted remarkable attention because of certain inherent advantages, including easy fabrication, simple device structure, low cost, and capability to be fabricated into light-weight, semitransparent and flexible devices.[1-8] In BHJ-OSCs, the photoactive layer is made of the blend of conjugated polymer or *p*-type organic semiconductor (*p*-OS) as donor and fullerene derivatives or *n*-type organic semiconductor (*n*-OS) as acceptor. In succession to the widely investigated fullerene derivatives,[9-13] a serious of *n*-OS acceptors with acceptor-donor-acceptor (A-D-A) structure are developed and synthesized because of their easily-tuned energy levels, wide and strong light absorption and diverse chemical structures.[8, 14, 15] And these non-fullerene OSCs show efficient charge generation upon small driving energies, resulting in high photocurrent and low voltage losses at the same time.[16-27] Consequently, power conversion efficiencies (PCEs) higher than 14% have been achieved in these non-fullerene OSCs.[28-31] The *n*-OS acceptors based on a fused-ring electron-donating core along with two strong electron-withdrawing end-groups have become dominant electron acceptor materials in high efficiency single-junction OSCs.

A planar ring-fused non-fullerene acceptor IDIC is one of noticeable *n*-OS acceptors, and high PCEs of over 11%[32-34] were realized in the IDIC-based polymer solar cells (PSCs). Besides, IDIC was also used in the non-fullerene all small molecule organic solar cells (SM-OSCs) with *p*-OS as donor and *n*-OS as acceptor and achieved excellent PCEs.[35-38]

The small molecule possesses advantages of well-defined molecular weight, easy purification and small batch-to-batch variation, which can show good reproducibility in device performance and provide reliable analyses of molecular properties and device performance relationship. Besides, small molecules have a lower viscosity and better structural order that can be used to manipulate the active layer morphology and performance.[5] Therefore, the solution-processed *p*-OS (or called organic small molecules) donor materials have also attracted great attention. Significant progress has been made with small molecule donors, and the OSCs with efficiencies over 10% were realized when they blended with fullerene acceptor materials.[12, 39-41] Naturally, the researchers could think to investigate the SM-OSCs in order to take dual advantages of both *p*-OS and *n*-OS. For example, Hou *et al*. reported a wide bandgap molecule DRTB-T with an alkythienyl-substituted benzodithiophene (BDT) trimer as the central unit and 3-ethyrhodanines as the end-capping groups; The DRTB-T:IDIC-based SM-OSCs obtained a PCE as high as 9.1%.[35] Then they designed a group of model compounds to demonstrate that the length of the end alkyl chain has great influence on the molecular orientation and photovoltaic performance; and a top PCE of up to 11.24% was achieved with a DRTB-T-C4:IT-4F-based device,

which is the highest value reported for SM-OSCs at that time.[42] Li *et al*. reported a series of wide bandgap small molecules based on benzodithiophene and ethyl cyanoacetic acid ester, H11[36], $BDT(TVT\text{-}SR)_2$[43], SM1[37] and H22[38]. By fine-tuning the π bridge unit and conjugated side chain of BDT, they all exhibited excellent photovoltaic performance, and the PCEs are 9.73%、11.1%、10.11% and 10.29%, respectively, when they blended with IDIC to construct SM-OSCs. The structure of these small molecule donors are listed in Fig. S1 in ESI† and their photovoltaic data are shown in Table S1 in ESI†. However, the PCEs of these SM-OSCs are still lower than non-fullerene PSCs, consistent efforts should be made to design and synthesize a suitable *p*-OS donor to combine with an *n*-OS acceptor to construct a high efficiency all-small-molecule system.

Considering various donor materials for solution processed OSCs with high photovoltaic performance, BDT is a promising building block for both polymers and small molecules due to its symmetric and planar conjugated structure.[11, 13, 27, 31, 44-49] In addition, the small molecules containing BDT as central building block also set new PCE records in SM-OSCs (Table S1, ESI†).[35-37, 42, 43] Therefore, the structure of BDT is chosen as a bridge to design a new small molecule donor material, which is different from previous ones (Fig. S1, ESI†). The small molecules with non-fused ring structures exhibited a good chain planarity and crystalline intermolecular organizations in film because of the non-covalent interaction, which is beneficial to the charge transfer and transmission.[50-52] Besides, the non-fused ring structure is very simple and synthesized easily, and the corresponding small molecule shows easily

adjustable absorption spectrum, molecular energy levels, and charge mobility by the simple chemical modification.[53] 3-ethylrhodanine has been widely used as a capping moiety to expand the conjugation and enhance the electron-accepting ability in the small molecule donors, which make it an efficient unit for high-performance OSCs.[35, 54] The presence of the ethyl group not only inhibits the hydrogen bonding associated with non-alkylated rhodanine, but also increases the solubility.

Based on the analysis mentioned above, we designed and synthesized a new small molecule P2TBR with thiophene-2, 5-bis ((2-ethylhexyl) oxy) benzene-thiophene (TBT) as central building block, 2D-conjugated benzo[1,2-b:4,5-b′]dithiophene (BDT) unit as π spacers and 3-ethylrhodanines as terminal groups. P2TBR possesses good solubility in common solvents and good thermal stability, which is beneficial for the device fabrication. IDIC having complementary absorption and matched energy level with P2TBR was chosen as acceptor for the SM-OSCs with P2TBR as donor. After fine tuning the morphology of the active layer with solvent vapor annealing (SVA), the SM-OSCs demonstrated an outstanding PCE of 11.5%, with a V_{oc} of 0.94 V, a J_{sc} of 17.5 mA cm^{-2}, and a satisfactory fill factor (FF) of 70.1%. To the best of our knowledge, the PCE of 11.5% is the highest value for non-fullerene SM-OSCs reported to date.

Results and discussion

Synthesis and properties of P2TBR

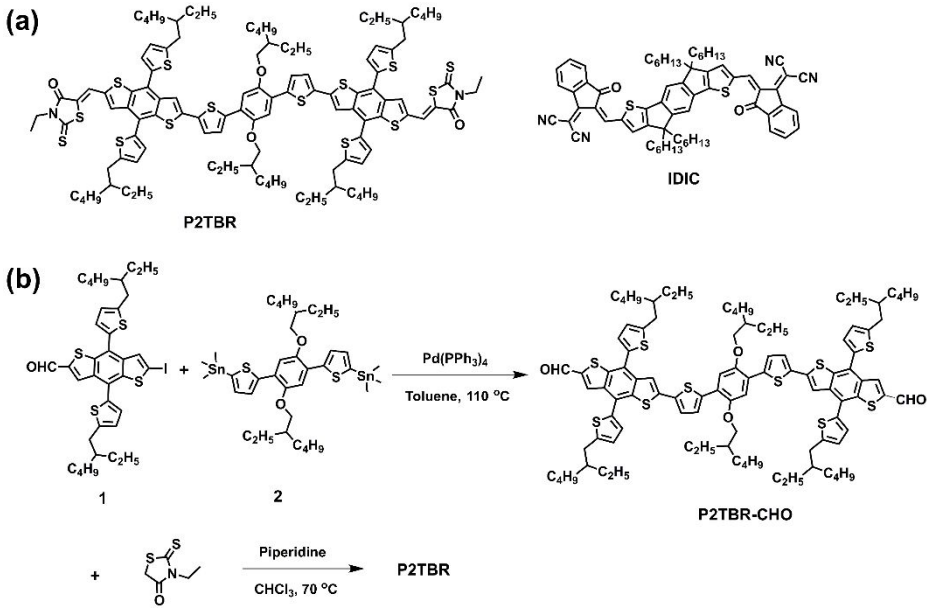

Fig. 1 (a) Chemical structures of *p*-OS donor P2TBR and *n*-OS acceptor IDIC. (b) Synthetic route of P2TBR.

The structure of *p*-OS donor P2TBR is shown in Fig. 1a, and the synthetic route is displayed in Fig. 1b. Compound **1** and **2** were prepared according to the reported literatures.[35, 55, 56] The intermediate compound P2TBR-CHO was synthesized through the Stille coupling reaction between compounds **1** and **2** using $Pd(PPh_3)_4$ as catalyst. Then a typical Knoevenagel condensation reaction of P2TBR-CHO with 3-ethylrhodanines afforded the target organic small molecule P2TBR. Detailed synthesis procedures are described in ESI†. The chemical structure of P2TBR was characterized using ^{1}H-NMR, ^{13}C-NMR, MALDI-TOF, and elemental analysis techniques in SI. The P2TBR exhibits good solubility in common organic solvents, such as chloroform (CF), chlorobenzene (CB) and *o*-dichlorobenzene (*o*-DCB) at room temperature, which is beneficial for the device fabrication. As shown in Fig. S2 in ESI†, thermogravimetric analysis (TGA) reveals that P2TBR possesses good

thermal stability with the thermal decomposition temperature (T_d) of 5% weight loss at 390 °C.

Density functional theory (DFT) calculations were used to gain the properties of P2TBR in the molecular electronic energy levels. The optimized molecular conformations and wavefunction distributions of the frontier orbitals of P2TBR are shown in Fig. S3 in ESI†. The electron density distributions at LUMO are localized on the entire molecule with higher density at the end groups, while the electron density distributions at HOMO are highly localized on the central core units. The BDT unit and terminal 3-ethylrhodanine moieties form a nearly flat plane and the dihedral angle is 0.81 °, the central TBT and BDT unit exhibit a dihedral angle of 6.03 °. The small dihedral angle means the small molecule P2TBR exhibits a highly coplanar conjugated backbone structure, which should be favorable for the π-π stacking and charge transport. P2TBR shows a relatively high hole mobility of 2.21 × 10^{-3} cm^2 V^{-1} s^{-1} (Fig. S4a, ESI†), which was measured via the space charge limited current (SCLC) method.[57]

Absorption spectra and electronic energy levels

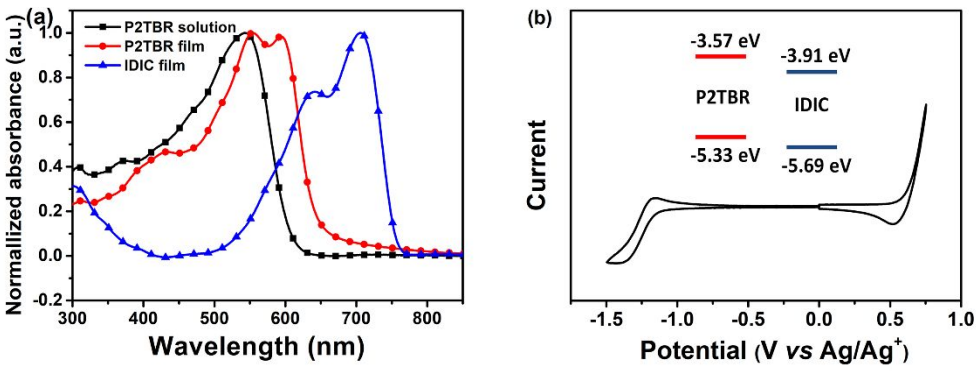

Fig. 2 (a) Normalized UV-vis absorption spectra of P2TBR solution and thin film and IDIC film. (b) Cyclic voltammogram of P2TBR film on a glassy carbon electrode in 0.1 mol L^{-1} Bu_4NPF_6 acetonitrile solution at a scan rate of 100 mV s^{-1} (calibrated by the Fc/Fc^+ redox couple).

Fig. 2a shows the normalized UV-vis absorption spectra of P2TBR in diluted chloroform ($CHCl_3$) solution and film. In solution, P2TBR exhibits absorption in the range of 300-620 nm with a maximum absorption peak (λ_{max}) at 543 nm. In thin films, the λ_{max} peak is red-shifted to 554 nm and a strong electronic vibration shoulder peak appeared at 594 nm, which is ascribed to the π-π* transition due to strong intermolecular π-π interactions in the solid state.[35] The optical band gap (E_g^{opt}) of P2TBR estimated from absorption onset (644 nm) is 1.93 eV, which is calculated from the equation of $E_g^{opt}=1240/\lambda_{onset}$. Cyclic voltammetry (CV) was conducted to investigate the frontier molecular orbital energy levels of P2TBR. From the CV plot in Fig. 2b, the corresponding HOMO and LUMO energy levels were determined to be -5.36 eV and -3.64 eV, respectively. The electronic energy levels of P2TBR as *p*-OS donor match well with that of *n*-OS acceptor IDIC (Fig. 2b), which should be able to afford enough driving force for charge separation.

Photovoltaic performance

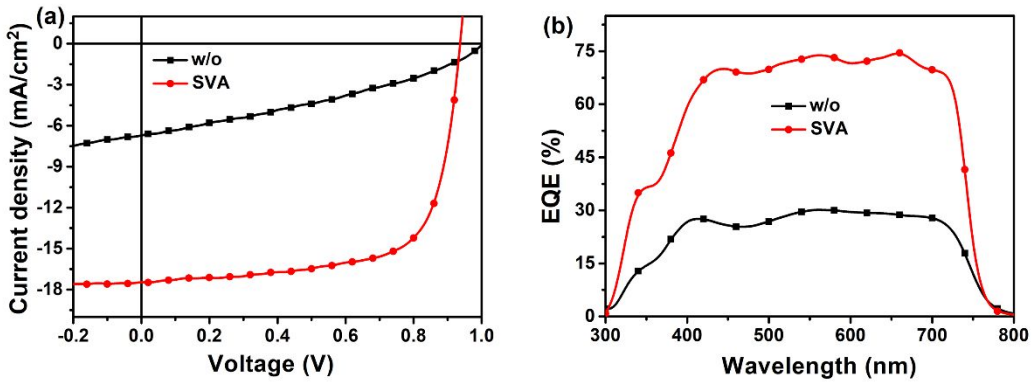

Fig. 3 (a) Current density-voltage (*J*-*V*) curves of the as-cast and optimal OSCs based on P2TBR:IDIC. (b) EQE curves of the corresponding OSCs.

Table 1 Photovoltaic performance of the OSCs based on P2TBR:IDIC (1:1, w/w) under the illumination of AM 1.5 G at 100 mW cm^{-2}.

P2TBR:IDIC	V_{oc} (V)	J_{sc}/J_{cal}[a] (m A cm^{-2})	FF (%)	PCE_{max}/PCE_{avg}[b] (%)
w/o	1.00	6.7 (6.6)	34.1	2.3 (2.2)
SVA[c]	0.94	17.5 (16.8)	70.1	11.5 (11.2)

[a]The calculated J_{sc} values from the EQE curves; [b]The average values of the PCE based on 20 devices are shown in brackets; [c]Solvent vapor annealing with CS_2.

IDIC possesses strong absorption between 500 and 800 nm, a suitable LUMO energy level (-3.91 eV) and a high electron mobility of about 1.10×10^{-3} cm^2 V^{-1} s^{-1}.[58] Thus, the combination of the *p*-OS P2TBR donor and the *n*-OS IDIC acceptor can afford broad absorption spectra and appropriate molecular energy levels, which are two key factors for realizing the efficient harvest of sunlight and the generation of free charges. BHJ all-small-molecule solar cells were fabricated with an conventional configuration of indium tin oxides

(ITO)/poly(3,4-ethylenendioxythiophene):poly(styrene sulfonate) (PEDOT:PSS)/P2TBR:IDIC/ZnO/Al, and characterized to investigate the photovoltaic performance of P2TBR. Chloroform was employed as the processing solvent, and the total concentration of donor and the acceptor was 14 mg mL^{-1} with a donor:acceptor (D/A) weight ratio of 1:1. The current density-voltage (*J*-*V*) curves and external quantum efficiency (EQE) spectra are shown in Fig. 3a, b, and the detailed photovoltaic parameters are summarized in Table 1. The as-cast devices showed inferior performance: V_{oc} of 1.00 V, J_{sc} of 6.7 mA cm^{-2}, FF of 34.1%, and PCE of 2.3%. The high V_{oc} is benefited from relatively low-lying HOMO energy levels of the *p*-OS donor P2TBR.

SVA has been proven to be a very effective route to control morphology and achieve promising enhancement in device performance.[35, 40, 59-61] Therefore, the morphology of P2TBR:IDIC blend film was optimized to further improve the device performance by SVA treatment. With the blend active layer processed by SVA with CS_2, the OSCs displayed a remarkably improved J_{sc} from 6.7 to 17.5 mA cm^{-2} and an obviously increased FF from 34.1% to 70.1% simultaneously, while the V_{oc} was slightly reduced to 0.94 V. The reduction in V_{oc} is found to originate from the charge recombination induced by the quasi-Fermi level variation between the donor and acceptor materials.[60] Finally, the champion PCE of 11.5% was achieved for the optimal device, which is the highest value reported for the all-small-molecule OSCs to date.

External quantum efficiency (EQE) tests were performed to verify their high J_{sc}

values and probe photo harvesting and charge collection processes of the OSCs. The calculated J_{sc} of the as-cast and optimal devices, integrated from their corresponding EQE curves, were 6.6 and 16.8 mA cm^{-2}, respectively, which agrees well with the J_{sc} values obtained from the *J-V* curves. Compared to the as-cast device, the optimal device shows higher EQE value in the whole wavelength range of absorption, indicating that both P2TBR and IDIC contributed greatly to the photocurrent. The EQE response of the optimal device reached over 70% in the range of *ca*. 440-700 nm and had a maximum value up to 74% at 660 nm (Fig. 3b). After SVA treatment, the hole and electron mobilities were estimated from SCLC method (Fig. S4b, c, ESI†) to be 3.54 × 10^{-4} and 3.34× 10^{-4} cm^2 V^{-1} s^{-1}, respectively, and the μ_h/μ_e was 1.06. The high and balanced μ_h/μ_e for the P2TBR:IDIC OSCs with SVA treatment is beneficial to suppress space charge accumulation and thus promote charge extraction, leading to its better J_{sc} and FF.

Exciton Dissociation and Charge Recombination

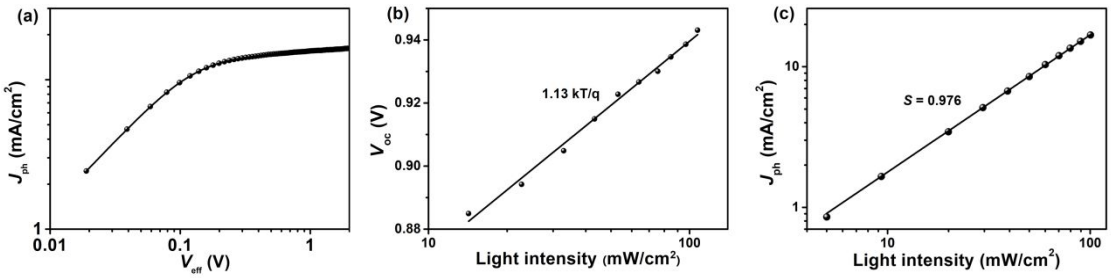

Fig. 4 (a) J_{ph}-V_{eff}, (b) V_{oc}-P and (c) J_{ph}-P curves of the optimal devices based on P2TBR:IDIC. The solid lines are the fitted lines in the V_{oc}-P and J_{ph}-P plots.

The dependence of the photocurrent density (J_{ph}) on the effective voltage (V_{eff})

was measured to evaluate the exciton dissociation and charge extraction efficiencies. J_{ph} is defined as J_L - J_D, where J_L and J_D are the photocurrent densities of the devices under illumination and in the dark, V_{eff} is defined as V_0 - V, where V_0 is voltage at which J_{ph} = 0 and V is the applied external voltage bias. Therefore, V_{eff} determines the electric field in the bulk region and thereby affects the carrier transport and the photocurrent extraction. At high V_{eff} values, mobile charge carriers rapidly move toward the corresponding electrodes with minimal recombination. The exciton dissociation probability (P_{diss}) can be estimated from the ratio of J_{ph}/J_{sat}; J_{sat} is the value where the J_{ph} reaches its saturation at high reverse voltage, which means all the photo-generated excitons are dissociated to free charge carriers and collected by the electrodes.[62] Under the short-circuit and maximum power output conditions, the P_{diss} were calculated to be 95.86% and 81.47% for the P2TBR:IDIC blend with SVA treatment, respectively (Fig. 4a), implying that the P2TBR:IDIC OSCs have an efficient exciton dissociation and charge extraction process, which is beneficial for realizing large J_{sc} and FF. The dependence of V_{oc} on light intensity (P_{light}) can be used to describe the order of the recombination process. The slope of V_{oc} versus ln P_{light} lines at 2 kT/q indicates that the dominant recombination mechanism is Shockley-Read-Hall or monomolecular recombination, while the slope of kT/q means that only bimolecular recombination take places in the devices (where k is the Boltzmann constant, T is the Kelvin temperature, q is the elementary charge).[63] As shown in Fig. 4b, the slope of 1.13 kT/q for the P2TBR:IDIC-based devices with SVA treatment is far from 2 kT/q and close to kT/q, which means that the dominant

recombination mechanism is bimolecular recombination. The dependence of J_{ph} on P was measured to further study the charge bimolecular recombination behavior under the short-circuit condition of the devices. The relationship between J_{ph} and P can be depicted by a power-law equation of $J_{ph} \propto P^S$, where the value of S indicates the degree of bimolecular recombination. It is generally assumed that if more free charges can be swept out and effectively collected in individual electrodes prior to recombination, the slope of S is closer to 1.[64] As shown in Fig. 4c, in logarithmic coordinates, the S value of the fitted lines was calculated as 0.976 for the devices based on P2TBR:IDIC blend films with SVA treatment. The higher S value indicates that there is very little charge carrier recombination in the device, which would reasonably enhance the utilization rate of excitons and improve the transport properties of carriers, facilitating the enhancement of J_{sc} and FF.

Film morphology

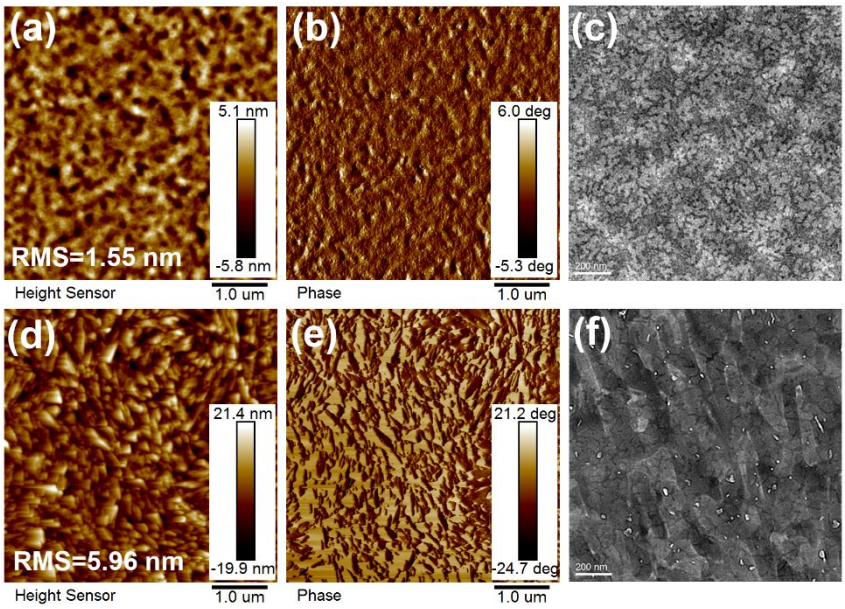

Fig. 5 AFM height (a, d), AFM phase (b, e) and TEM images (c, f) for the as-cast blend film (a, b, c) and optimal blend film (d, e, f) based on P2TBR:IDIC.

Morphology of the active layer is a critical factor to determine the photovoltaic performance of the OSCs.[65-70] The big difference in the morphology is supposed to be the main reason for the different PCEs of the P2TBR:IDIC OSCs. The Atomic force microscopy (AFM) and transmission electron microscopy (TEM) were carried out to investigate the surface and bulk morphlogy of the active layers and understand the relationship between the evolution of the active layer morphology and device performance. In the AFM images (Fig. 5a, b), the P2TBR:IDIC blend film presented uniform and smooth feature with a relatively small root-mean-square (RMS) roughness of 1.55 nm. After SVA treatment, the RMS roughness of the blend film dramatically incaresed to 5.96 nm and exhibited apparent aggregation feature (Fig. 5d, e). The large RMS roughness is similar to some reported all-small-molecule systems (H11:IDIC, RMS = 6.94 nm[71]; DRTB-T:IDIC, RMS = 5.75 nm[35]), all of them possess relatively high PCEs. The RMS values of the all-small-molecule blend films are generally larger than those of the polymer based blend film. And the big difference of the RMS may be due to the stronger self-aggregation of the OSs with the lower entropy barrier.[36] The result suggests that SVA treatment induced the aggregation of P2TBR and IDIC in the blend film. The TEM image clearly showed large morphological changes upon SVA treatment, which agreed well with the AFM morphology observations.

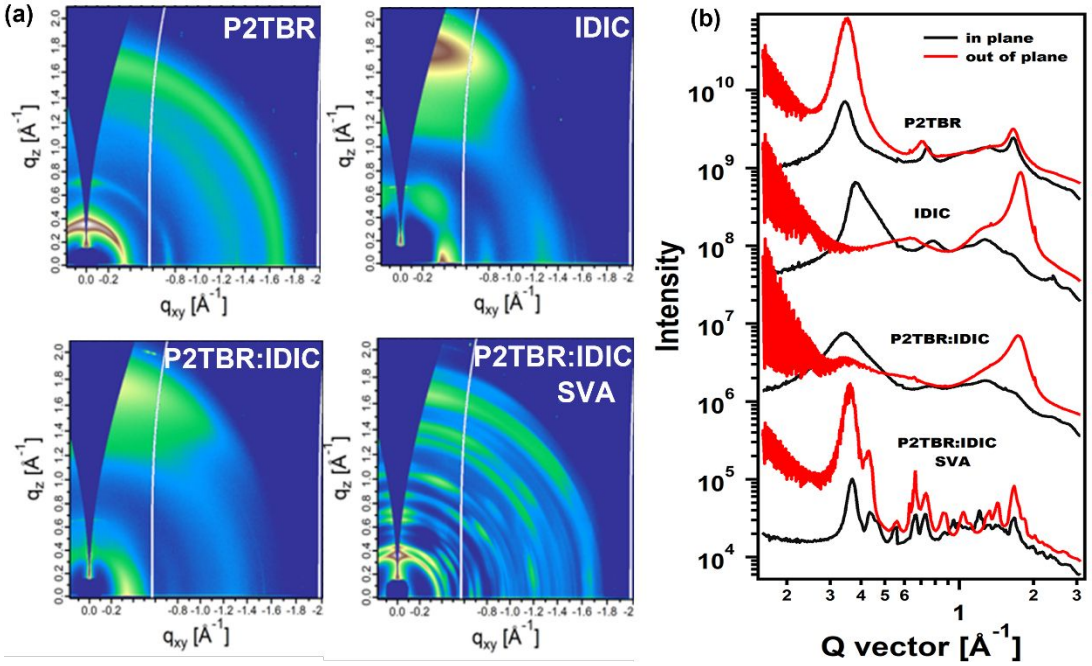

Fig. 6 (a) 2D GIWAXS images of neat and blend films. (b) The corresponding in-plane (q_{xy}) (black line) and out-of-plane (q_z) (red line) cut profiles.

The molecular packing and texture of the neat and blend films were investigated by grazing-incidence wide-angle X-ray scattering (GIWAXS).[72] The diffraction images and the related in-plane (IP) and out-of-plane (OOP) line-cut profiles are displayed in Fig. 6. P2TBR neat film shows a complicated molecular ordering. There is a pronounced (100) laminar packing diffraction peak at 0.34 Å^{-1} in both IP and OOP direction. Meanwhile, the (010) π-π stacking peak at 1.66 Å^{-1} in IP and OOP direction is also observed, indicating that P2TBR has both edge-on and face-on crystalline orientaion. IDIC neat film shows a predominant face-on orentation relative to the substrate, as evidenced by the (100) peak at 0.38 Å^{-1} in the IP direction and strong π-π stacking peak at 1.77 Å^{-1} in the OOP direction (Fig. 6a, b). These structure features

remain in BHJ blends. As seen from the as-cast blend film, P2TBR (100) diffraction peak at 0.34 $Å^{-1}$ can be clearly observed in IP patterns with a broad azimuthal angle spreading. The π-π stacking peak area is dominated by that of IDIC, centered at 1.74 $Å^{-1}$, which is slightly away from that of the neat thin film. This indicates a favoured face-on orientation relative to the substrate. SVA can effectively change the structure order of the BHJ blend film, leading to great changes of scattering features. As seen from Fig. 6a, b, some new and weak scttering spots are present in the 2D GIWAXS plots upon SVA treatment, indicating that larger crystallization were formed. Notably, a diffraction peak at 0.43 $Å^{-1}$ is seen in both IP and OOP direction. A clear texture comprising of face-on and edge-on crystallites were observed in the SVA film, indicating the co-existence of vertical and parallel charge transportation channel in a sandwich device structure. In 2016, Yang *et al.* reported for the first time that a mixed face-on and edge-on texture was far better than that of the face-on orientated host film in ternary blend comprising PTB7-Th:DR3TSBDT:$PC_{71}BM$.[73] Similar texture feature is also disclosed in high efficiency SM-OSCs.[35, 36, 74] Therefore, compared to the as-cast P2TBR:IDIC film with face-on orientation, the SVA film displays better crystallization property and three dimensional charge pathways, which is beneficial to intermolecualr charge transfer.

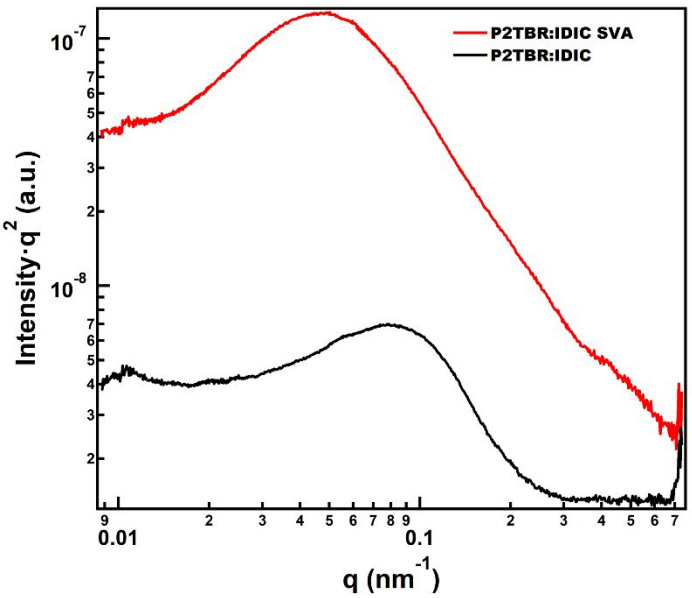

Fig. 7 R-SoXS scattering profiles of the P2TBR:IDIC blend films.

Phase separation of blend films was studied using resonant soft X-ray scattering (R-SoXS).[75-77] X-ray with photon energy of 284.2 eV was selected to enhance material contrast.[78, 79] As shown in Fig. 7, the BHJ thin film with SVA treatment led to obvious R-SoXS intensity enhancement, indicating that the phase separation is better developed. R-SoXS can also reveal the average composition variations (relative domain purity) via integrating scattering profiles. The higher total scattering intensity (TSI) implies the purer average domains.[80] Upon SVA treatment, the domain purity of the device is improved because of broadened scattering profile and enhanced scattering intensity, which is in agreement with the AFM and TEM results. It is beneficial to suppress bimolecular recombination and promote charge collection and extraction. Combined the GIWAXS and R-SoXS analysis of P2TBR:IDIC system without and with SVA treatment, we can see SVA treatment can improve crystallinity

and enhance phase purity of blend films. It is favorable for increasing FF, thereby higher PCEs after SVA treatment were obtained.

Fig. S5 gives the PCEs of P2TBR gained in this work and the other high efficiency small molecule donors which show PCEs of over 9% in SM-OSCs (Fig. S1 and Table S1 for the details in ESI†). It is easy to find that these small molecule donors all contain BDT central building block, while P2TBR has the non-fused ring (TVT) core. As previously stated, the non-fused ring molecule with non-covalent interaction has many advantages, such as good planarity, high crystallinity, easy chemical modificaiton. In this work, the small molecule P2TBR posses a state-of-the-art PCE of 11.5% in SM-OSCs, and the value is the highest PCE reported so far. Therefore, the exciting results further indicate that the non-fused ring stucture is a good unit to use in the high efficiency organic small moelcule donors.

Conclusions

In conclusion, a new small molecule P2TBR with non-fused TBT as central unit, BDT as conjugated π spacers and 3-ethylrhodanines as terminal groups was developed and used as a donor material in non-fullerene SM-OSCs. P2TBR shows strong absorption, low-lying HOMO energy level, high hole mobility and good thermal stability. The P2TBR:IDIC based OSCs with solvent vapor annealing treatment by CS_2 exhibited an outstanding PCE of 11.5%, with a V_{oc} of 0.94 V, a J_{sc} of 17.5 mA cm^{-2}, and a FF of 70.1%. This efficiency is the highest PCE for non-fullerene all-small-molecule systems reported to date. In a word, the results

indicate that P2TBR is a promising candidate of *p*-OS donor materials in SM-OSCs, and the molecular design strategy for P2TBR gives a guideline that the simple-structured and easy chemical modification non-fused unit can be also used as building blocks in high performation *p*-OS donors.

Conflicts of interest

There are no conflicts to declare.

Acknowledgements

This work was supported by National Natural Science Foundation of China (NSFC) (No. 51503135, 51573120, 51773142, 21704082, 21875182 and 91633301), Ministry of science and technology (No. 2016YFA0200700), Jiangsu Provincial Natural Science Foundation (No. BK20150332). The X-ray data was acquired at beamlines 7.3.3 and 11.0.1.2 at the Advanced Light Source, which is supported by the Director, Office of Science, Office of Basic Energy Sciences, of the U.S. Department of Energy under Contract No. DE-AC02-05CH11231. The authors thank Chenhui Zhu at beamline 7.3.3, and Cheng Wang at beamline 11.0.1.2 for assistance with data acquisition.

Notes and References

1 H. Hoppe and N. S. Sariciftci, *J. Mater. Res.*, 2011, **19**, 1924-1945.

2 M. C. Scharber and N. S. Sariciftci, *Prog. Polym. Sci.*, 2013, **38**, 1929-1940.

3 M. E. Ragoussi and T. Torres, *Chem. Commun. (Camb)*, 2015, **51**, 3957-3972.

4 L. Lu, T. Zheng, Q. Wu, A. M. Schneider, D. Zhao and L. Yu, *Chem. Rev.*, 2015, **115**, 12666-12731.

5 Y. Lin, Y. Li and X. Zhan, *Chem. Soc. Rev.*, 2012, **41**, 4245-4272.

6 Y. S. Chen, X. J. Wan, G. K. Long. *Acc. Chem. Res.* 2013, **46**, 2645-2655.

7 A. Polman, M. Knight, E. C. Garnett, B. Ehrler and W. C. Sinke, *Science*, 2016, **352**, aad4424.

8 J. Hou, O. Inganas, R. H. Friend and F. Gao, *Nat. Mater.*, 2018, **17**, 119-128.

9 Z. Hu, L. Ying, F. Huang and Y. Cao, *Sci. China Chem.*, 2017, **60**, 571-582.

10 J. Zhao, Y. Li, G. Yang, K. Jiang, H. Lin, H. Ade, W. Ma and H. Yan, *Nat. Energy*, 2016, **1**, 15027.

11 D. Zhu, X. Bao, D. Ouyang, J. Wang, X. Yuan, Q. Wang, D. Zhou, S. Wen and R. Yang, *Nano Energy*, 2017, **40**, 495-503.

12 D. Deng, Y. Zhang, J. Zhang, Z. Wang, L. Zhu, J. Fang, B. Xia, Z. Wang, K. Lu, W. Ma and Z. Wei, *Nat. Commun.*, 2016, **7**, 13740.

13 Z. Zhang, Z. Zhang, B. Zhao, Y. Huang, J. Xiong, P. Cai, X. Xue, J. Zhang and S. Tan, *J. Mater. Chem. A*, 2018, **6**, 12969-12973.

14 Y. Yang, Z. G. Zhang, H. Bin, S. Chen, L. Gao, L. Xue, C. Yang and Y. Li, *J. Am. Chem. Soc.*, 2016, **138**, 15011-15018.

15 S. Li, W. Liu, C. Z. Li, M. Shi and H. Chen, *Small*, 2017, **13**, 1701120.

16 B. Huang, L. Chen, X. Jin, D. Chen, Y. An, Q. Xie, Y. Tan, H. Lei and Y. Chen, *Adv. Funct. Mater.*, 2018, **28**, 1800606.

17 Q. P. Fan, Z. Xu, X. Guo, X. Y. Meng, W. B. Li, W. Y. Su, X. M. Ou, W. Ma, M. J. Zhang and Y. F. Li, *Nano Energy*, 2017, **40**, 20-26.

18 Y. Wang, Q. P. Fan, X. Guo, W. B. Li, B. Guo, W. Y. Su, X. M. Ou and M. J. Zhang, *J. Mater. Chem. A*, 2017, **5**, 22180-22185.

19 J. Liu, S. S. Chen, D. P. Qian, B. Gautam, G. F. Yang, J. B. Zhao, J. Bergqvist, F. L. Zhang, W. Ma, H. Ade, O. Inganas, K. Gundogdu, F. Gao and H. Yan, *Nat. Energy*, 2016, **1**, 16089.

20 D. Baran, T. Kirchartz, S. Wheeler, S. Dimitrov, M. Abdelsamie, J. Gorman, R. S. Ashraf, S. Holliday, A. Wadsworth, N. Gasparini, P. Kaienburg, H. Yan, A. Amassian, C. J. Brabec, J. R. Durrant and I. McCulloch, *Energy Environ. Sci*, 2016, **9**, 3783-3793.

21 H. Bin, L. Gao, Z. G. Zhang, Y. Yang, Y. Zhang, C. Zhang, S. Chen, L. Xue, C. Yang, M. Xiao and Y. Li, *Nat. Commun.*, 2016, **7**, 13651.

22 S. Chen, Y. Liu, L. Zhang, P. C. Y. Chow, Z. Wang, G. Zhang, W. Ma and H. Yan, *J. Am. Chem. Soc.*, 2017, **139**, 6298-6301.

23 P. Cheng, M. Zhang, T. K. Lau, Y. Wu, B. Jia, J. Wang, C. Yan, M. Qin, X. Lu and X. Zhan, *Adv. Mater.*, 2017, **29**, 1605216.

24 M. Privado, P. de la Cruz, S. Biswas, R. Singhal, G. D. Sharma, F. Langa, *J. Mater. Chem. A*, 2018, **6**, 11714-11724.

25 Q. Fan, Z. Xu, X. Guo, X. Meng, W. Li, W. Su, X. Ou, W. Ma, M. Zhang and Y. Li, *Nano Energy*, 2017, **40**, 20-26.

26 Y. Wang, Q. Fan, X. Guo, W. Li, B. Guo, W. Su, X. Ou and M. Zhang, *J. Mater.*

Chem. A, 2017, **5**, 22180-22185.

27 W. Gao, T. Liu, R. Ming, Z. Luo, K. Wu, L. Zhang, J. Xin, D. Xie, G. Zhang, W. Ma, H. Yan and C. Yang, *Adv. Funct. Mater.*, 2018, **28**, 1803128.

28 H. Zhang, H. Yao, J. Hou, J. Zhu, J. Zhang, W. Li, R. Yu, B. Gao, S. Zhang and J. Hou, *Adv. Mater.*, 2018, **30**, 1800613.

29 Y. Zhang, H. Yao, S. Zhang, Y. Qin, J. Zhang, L. Yang, W. Li, Z. Wei, F. Gao and J. Hou, *Sci. China Chem.*, 2018, **61**, 1328-1337.

30 B. Kan, H. Feng, H. Yao, M. Chang, X. Wan, C. Li, J. Hou and Y. Chen, *Sci. China Chem.*, 2018, **61**, 1307-1313..

31 S. Zhang, Y. Qin, J. Zhu and J. Hou, *Adv. Mater.*, 2018, **30**, 1800868.

32 Y. Lin, F. Zhao, S. K. K. Prasad, J. D. Chen, W. Cai, Q. Zhang, K. Chen, Y. Wu, W. Ma, F. Gao, J. X. Tang, C. Wang, W. You, J. M. Hodgkiss and X. Zhan, *Adv. Mater.*, 2018, **30**, 1706363.

33 J. D. Chen, Y. Q. Li, J. Zhu, Q. Zhang, R. P. Xu, C. Li, Y. X. Zhang, J. S. Huang, X. Zhan, W. You and J. X. Tang, *Adv. Mater.*, 2018, **30**, 1706083.

34 Q. Fan, Y. Wang, M. Zhang, B. Wu, X. Guo, Y. Jiang, W. Li, B. Guo, C. Ye, W. Su, J. Fang, X. Ou, F. Liu, Z. Wei, T. C. Sum, T. P. Russell and Y. Li, *Adv. Mater.*, 2018, **30**, 1704546.

35 L. Yang, S. Zhang, C. He, J. Zhang, H. Yao, Y. Yang, Y. Zhang, W. Zhao and J. Hou, *J. Am. Chem. Soc.*, 2017, **139**, 1958-1966.

36 H. Bin, Y. Yang, Z. G. Zhang, L. Ye, M. Ghasemi, S. Chen, Y. Zhang, C. Zhang, C. Sun, L. Xue, C. Yang, H. Ade and Y. Li, *J. Am. Chem. Soc.*, 2017, **139**,

5085-5094.

37 B. Qiu, L. Xue, Y. Yang, H. Bin, Y. Zhang, C. Zhang, M. Xiao, K. Park, W. Morrison, Z.-G. Zhang and Y. Li, *Chem. Mater.*, 2017, **29**, 7543-7553.

38 H. Bin, J. Yao, Y. Yang, I. Angunawela, C. Sun, L. Gao, L. Ye, B. Qiu, L. Xue, C. Zhu, C. Yang, Z. G. Zhang, H. Ade and Y. Li, *Adv. Mater.*, 2018, **30**, 1706361.

39 J. Wan, X. Xu, G. Zhang, Y. Li, K. Feng and Q. Peng, *Energy Environ. Sci.*, 2017, **10**, 1739-1745.

40 B. Kan, M. Li, Q. Zhang, F. Liu, X. Wan, Y. Wang, W. Ni, G. Long, X. Yang, H. Feng, Y. Zuo, M. Zhang, F. Huang, Y. Cao, T. P. Russell and Y. Chen, *J. Am. Chem. Soc.*, 2015, **137**, 3886-3893.

41 M. Li, K. Gao, X. Wan, Q. Zhang, B. Kan, R. Xia, F. Liu, X. Yang, H. Feng, W. Ni, Y. Wang, J. Peng, H. Zhang, Z. Liang, H.-L. Yip, X. Peng, Y. Cao and Y. Chen, *Nat. Photon.*, 2016, **11**, 85-90.

42 L. Yang, S. Zhang, C. He, J. Zhang, Y. Yang, J. Zhu, Y. Cui, W. Zhao, H. Zhang, Y. Zhang, Z. Wei and J. Hou, *Chem. Mater.*, 2018, **30**, 2129-2134.

43 J. Guo, H. Bin, W. Wang, B. Chen, J. Guo, R. Sun, Z.-G. Zhang, X. Jiao, Y. Li and J. Min, *J. Mater. Chem. A*, 2018, **6**, 15675-15683.

44 Q. Fan, W. Su, Y. Wang, B. Guo, Y. Jiang, X. Guo, F. Liu, T. P. Russell, M. Zhang, Y. Li, *Sci. China Chem.*, 2018, **61**, 531-537.

45 W. Zhao, S. Li, H. Yao, S. Zhang, Y. Zhang, B. Yang and J. Hou, *J. Am. Chem. Soc.*, 2017, **139**, 7148-7151.

46 X. Xu, T. Yu, Z. Bi, W. Ma, Y. Li and Q. Peng, *Adv. Mater.*, 2018, **30**, 1703973.

47 Z. Fei, F. D. Eisner, X. Jiao, M. Azzouzi, J. A. Rohr, Y. Han, M. Shahid, A. S. R. Chesman, C. D. Easton, C. R. McNeill, T. D. Anthopoulos, J. Nelson and M. Heeney, *Adv. Mater.*, 2018, **30**, 1705209.

48 W. Zhao, S. Zhang, Y. Zhang, S. Li, X. Liu, C. He, Z. Zheng and J. Hou, *Adv. Mater.*, 2018, **30**, 1704837.

49 Q. Wan, X. Guo, Z. Wang, W. Li, B. Guo, W. Ma, M. Zhang and Y. Li, *Adv. Funct. Mater.*, 2016, **26**, 6635-6640.

50 S. Li, L. Zhan, F. Liu, J. Ren, M. Shi, C. Z. Li, T. P. Russell and H. Chen, *Adv. Mater.*, 2018, **30**, 1705208.

51 O. K. Kwon, J.-H. Park, S. K. Park and S. Y. Park, *Adv. Energy Mater.*, 2015, **5**, 1400929.

52 O. K. Kwon, M. A. Uddin, J. H. Park, S. K. Park, T. L. Nguyen, H. Y. Woo and S. Y. Park, *Adv. Mater.*, 2016, **28**, 910-916.

53 S. Li, L. Zhan, W. Zhao, S. Zhang, B. Ali, Z. Fu, T.-K. Lau, X. Lu, M. Shi, C.-Z. Li, J. Hou and H. Chen, *J. Mater. Chem. A*, 2018, **6**, 12132-12141.

54 H. Li, Y. Zhao, J. Fang, X. Zhu, B. Xia, K. Lu, Z. Wang, J. Zhang, X. Guo and Z. Wei, *Adv. Energy Mater.*, 2018, **8**, 1702377.

55 H. Guo, T. Shen, F. Wu, R. Hou, X. Liu, B. Zhao, *J. Appl. Polym. Sci.*, 2016, **133**, 42982.

56 X.-Q. Chen, X. Yao, T. Bai, J. Ling, W.-J. Xiao, J. Wang, S.-C. Wu, L.-N. Liu, G. Xie, J. Li, Z. Lu, I. Visoly-Fisher, E. A. Katz and W.-S. Li, *J. Polym. Sci.,*

Part A: Polym. Chem., 2018, **56**, 689-698.

57 P. W. M. Blom, M. J. M. de Jong and J. J. M. Vleggaar, *Appl. Phys. Lett.*, 1996, **68**, 3308-3310.

58 Y. Lin, Q. He, F. Zhao, L. Huo, J. Mai, X. Lu, C. J. Su, T. Li, J. Wang, J. Zhu, Y. Sun, C. Wang and X. Zhan, *J. Am. Chem. Soc.*, 2016, **138**, 2973-2976.

59 K. Gao, W. Deng, L. Xiao, Q. Hu, Y. Kan, X. Chen, C. Wang, F. Huang, J. Peng, H. Wu, X. Peng, Y. Cao, T. P. Russell and F. Liu, *Nano Energy*, 2016, **30**, 639-648.

60 B. Xiao, M. Zhang, J. Yan, G. Luo, K. Gao, J. Liu, Q. You, H.-B. Wang, C. Gao, B. Zhao, X. Zhao, H. Wu and F. Liu, *Nano Energy*, 2017, **39**, 478-488.

61 M. Li, F. Liu, X. Wan, W. Ni, B. Kan, H. Feng, Q. Zhang, X. Yang, Y. Wang, Y. Zhang, Y. Shen, T. P. Russell and Y. Chen, *Adv. Mater.*, 2015, **27**, 6296-6302.

62 P. W. M. Blom, V. D. Mihailetchi, L. J. A. Koster and D. E. Markov, *Adv. Mater.*, 2007, **19**, 1551-1566.

63 A. K. K. Kyaw, D. H. Wang, V. Gupta, W. L. Leong, L. Ke, G. C. Bazan and A. J. Heeger, *ACS Nano*, 2013, **7**, 4569-4577.

64 S. R. Cowan, A. Roy and A. J. Heeger, *Phys. Rev. B*, 2010, **82**, 245207..

65 R.-Z. Liang, M. Babics, A. Seitkhan, K. Wang, P. B. Geraghty, S. Lopatin, F. Cruciani, Y. Firdaus, M. Caporuscio, D. J. Jones and P. M. Beaujuge, *Adv. Funct. Mater.*, 2018, **28**, 1705464.

66 F. Zhao, C. Wang and X. Zhan, *Adv. Energy Mater.*, 2018, **8**, 1703147.

67 S. Chen, Y. An, G. K. Dutta, Y. Kim, Z.-G. Zhang, Y. Li and C. Yang, *Adv.*

Funct. Mater., 2017, **27**, 1603564.

68 M. Jeong, S. Chen, S. M. Lee, Z. Wang, Y. Yang, Z.-G. Zhang, C. Zhang, M. Xiao, Y. Li and C. Yang, *Adv. Energy Mater.*, 2018, **8**, 1702166.

69 S. Chen, H. J. Cho, J. Lee, Y. Yang, Z.-G. Zhang, Y. Li and C. Yang, *Adv. Energy Mater.*, 2017, **7**, 1701125.

70 S. Chen, S. M. Lee, J. Xu, J. Lee, K. C. Lee, T. Hou, Y. Yang, M. Jeong, B. Lee, Y. Cho, S. Jung, J. Oh, Z.-G. Zhang, C. Zhang, M. Xiao, Y. Li and C. Yang, *Energy Environ. Sci.*, 2018, **11**, 2569-2680.

71 H. Bin, Y. Yang, Z.-G. Zhang, L. Ye, M. Ghasemi, S. Chen, Y. Zhang, C. Zhang, C. Sun, L. Xue, C. Yang, H. Ade and Y. Li, *J. Am. Chem. Soc.*, 2017, **139**, 5085-5094.

72 A. Hexemer, W. Bras, J. Glossinger, E. Schaible, E. Gann, R. Kirian, A. MacDowell, M. Church, B. Rude and H. Padmore, *J. Phys. Conf. Ser.*, 2010, **247**, 012007.

73 T. Kumari, S. M. Lee, S.-H. Kang, S. Chen and C. Yang, *Energy Environ. Sci.*, 2017, **10**, 258-265.

74 S. Badgujar, C. E. Song, S. Oh, W. S. Shin, S.-J. Moon, J.-C. Lee, I. H. Jung and S. K. Lee, *J. Mater. Chem. A*, 2016, **4**, 16335-16340.

75 S. Swaraj, C. Wang, H. Yan, B. Watts, J. Luning, C. R. McNeill and H. Ade, *Nano Lett.*, 2010, **10**, 2863-2869.

76 W. Ma, J. R. Tumbleston, L. Ye, C. Wang, J. Hou and H. Ade, *Adv. Mater.*, 2014, **26**, 4234-4241.

77 W. Ma, J. R. Tumbleston, M. Wang, E. Gann, F. Huang and H. Ade, *Adv. Energy Mater.*, 2013, **3**, 864-872.

78 Y. Wu, Z. Wang, X. Meng, W. Ma, *Prog. Chem.*, 2017, **29**, 93-101.

79 E. Gann, A. T. Young, B. A. Collins, H. Yan, J. Nasiatka, H. A. Padmore, H. Ade, A. Hexemer and C. Wang, *Rev. Sci. Instrum.*, 2012, **83**, 045110.

80 W. Ma, L. Ye, S. Zhang, J. Hou and H. Ade, *J. Mater. Chem. C*, 2013, **1**, 5023-5030.

The table of contents entry

All-small-molecule OSCs based on a new small molecule P2TBR with non-fused ring core exhibited record-breaking PCE of 11.5%.